19th International Conference on
Adaptive Structures and Technologies
October 6-9, 2008
Ascona, Switzerland

ACTIVE FLUTTER CONTROL OF A SMART FIN

Fatih Mutlu Karadal[+,1,2], Volkan Nalbantoğlu[†,1], Melin Şahin[‡,1], Güçlü Seber[',1], Ömer Faruk Kırcalı[",1,3], Yavuz Yaman[*,1]

[1] Department of Aerospace Engineering, Middle East Technical University, Ankara, TURKEY
[2] TAI, Turkish Aerospace Industries, Inc., Ankara, TURKEY
[3] STM, Defence Technologies Inc., Ankara, TURKEY

[+]Aerospace Engineer, M. Sc., e-mail: fkaradal@tai.com.tr
[†]Instruc. Dr., e-mail: volkan@ae.metu.edu.tr
[‡]Assist. Prof. Dr., e-mail: msahin@metu.edu.tr
'Instruc. Dr., e-mail: gseber@ae.metu.edu.tr
"Aerospace Engineer, M. Sc., e-mail: fkircali@stm.com.tr
[*]Prof. Dr., e-mail: yyaman@metu.edu.tr

ABSTRACT

This study presents the theoretical analysis of an active flutter suppression methodology applied on a smart fin. The smart fin consisted of a cantilever aluminum plate-like structure with surface bonded piezoelectric (PZT, Lead- Zirconate-Titanate) patches. The robust controllers were designed via H_∞ synthesis by considering both SISO (Single-Input, Single-Output) and MIMO Multi-Input, Multi-Output) aeroelastic system models. The developed controllers performed well around the flutter point and also stabilized the system over a wide flow speed range.

Keywords: Active flutter control, piezoelectricity, smart structure, H_∞ controller design

1. INTRODUCTION

There have been intensive efforts to understand the aeroelastic behavior of structures more accurately in order to avoid catastrophic structural failure due to excessive vibrations. Since current aircraft designs move toward lighter structures to improve the fuel efficiency and aircraft agility, various aeroelastic problems are likely to occur more frequently. In recent years, extensive research has been carried out to develop methodologies for controlling the aeroelastic behavior of structures.

Flutter suppression is one of the main objectives of the aeroelastic control. Flutter is a self-excited oscillation of a structure caused by the interaction of the aerodynamic, inertial and elastic characteristics of the components involved. At speeds below the flutter speed, oscillations will be damped. At the flutter speed, oscillations will persist with constant amplitude (zero damping). At speeds above the flutter speed, oscillations will diverge and hence cause the damage to or destruction of the structure.

In recent years, applications of smart structures in active control of aeroelastic systems have been studied in order to favorably modify the flutter behavior of aeroelastic systems. An analytical and experimental investigation of flutter suppression of a fixed wing by piezoelectric actuators was performed by Heeg [1] with the corresponding experimental studies performed at NASA Langley

Research Center under the Piezoceramic Aeroelastic Response Tailoring Investigation (PARTI) program. Experimental results indicated that significant flutter suppression was achieved. Döngi *et al.* [2] presented a finite element method based on numerical solution for flutter suppression of adaptive panel with self-sensing piezoelectric actuators in high supersonic flow. In one of the recent studies, Han *et al.* [3] presented a numerical and experimental investigation on active flutter suppression of a swept-back lifting surface using piezoelectric actuation. H_2- and μ–synthesized robust control laws were designed for flutter suppression and the performances of the two control methods were compared.

This paper investigates active flutter control of a smart fin using piezoelectric actuation. The aeroelastic model of the smart fin was determined in the state-space representation form using finite element method, panel aerodynamic method and rational function approximation. The unsteady aerodynamic loads acting on the structure were calculated by using Doublet-Lattice Method available in MSC®/NASTRAN/Aeroelasticity I. These aerodynamic loads were approximated as rational functions of the Laplace variable by using one of the aerodynamic approximation schemes, Roger's approximation, with least-squares method. The approximated aerodynamic loads together with the structural matrices, vibration and piezoelectric actuation characteristics obtained by finite element method were used to construct the state-space representation of the aeroelastic model for the smart fin. The obtained state-space model enabled to analyze the system and to design and develop the controllers.

H_∞-synthesized controllers were designed by considering SISO and MIMO aeroelastic system models. The performances of the controllers in vibration suppression and the enhancement in the flutter boundary of the smart fin were investigated.

2. DESCRIPTION OF THE SMART FIN

The smart fin consists of a cantilever aluminum passive plate-like structure with symmetrically surface bonded twenty-four piezoelectric actuator patches (25mm x 25mm x 0.5mm, Sensortech BM500 type). The actual system and the model of the smart fin showing the placement of the actuators are shown in Figure 2.1. The material properties of the aluminum plate are: E = 69 GPa, $\nu = 0.33$ and $\rho = 2768$ kg/m^3 and the thickness of the plate is 0.93 mm. The electromechanical properties of the piezoelectric patches are given in Appendix.

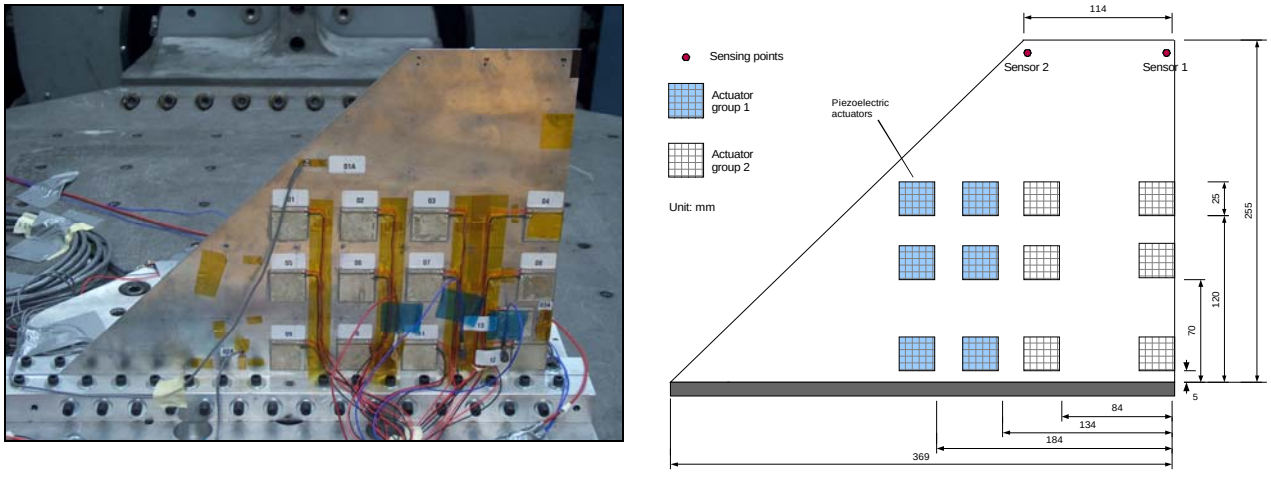

Figure 2.1 (a) The smart fin used in the study (b) the model of the smart fin

3. NUMERICAL MODEL

Figure 3.1 shows the flowchart for the numerical modeling procedure used in the study. With given geometry and material properties of the smart structure, the finite element model is formed and the structural matrices and vibration characteristics are obtained by using the finite element analysis. The thermal analogy method, in which the analogy between piezoelectric strain and thermally induced strain is used to allow temperature changes to model piezoelectric voltage actuation, is applied in the finite element analysis in order to obtain piezoelectric actuation properties. The structural and aerodynamic models of the smart fin are connected with splines. This model together with the vibration characteristics are used to obtain the unsteady aerodynamics in tabular form for various airflow parameters. The Roger's approximation and least-square method are applied to convert the unsteady aerodynamics into Laplace domain aerodynamics. A state-space system is constructed by integrating structural matrices, vibration and actuation characteristics of the smart fin, and the resulting aerodynamics. This section outlines these individual numerical procedures.

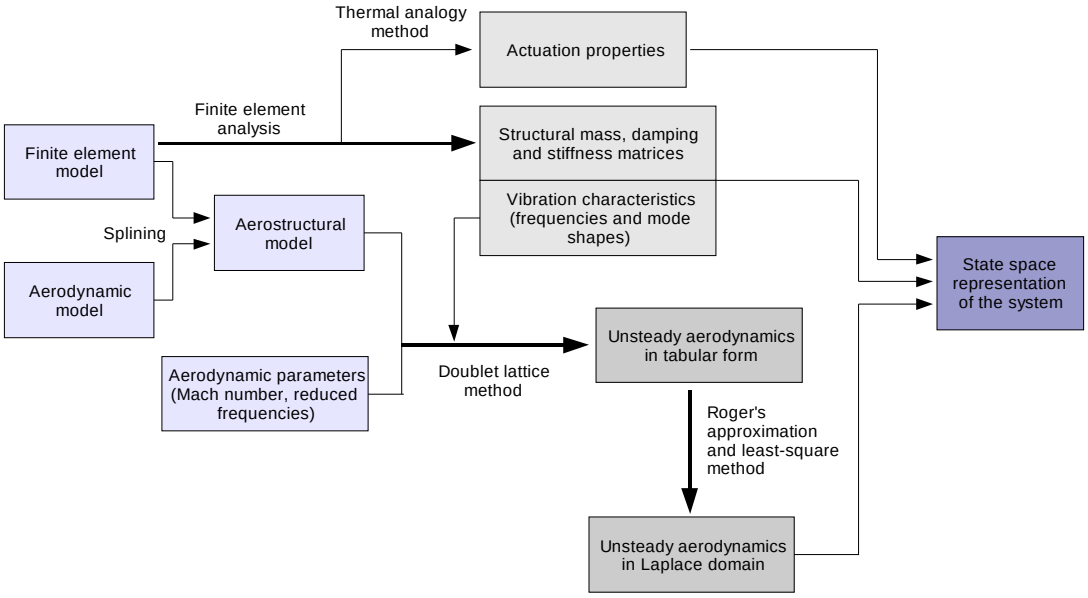

Figure 3.1 Flowchart of the numerical procedure used in the study

3-1. Structural Model

The governing equation of motion of a smart structure subjected to the piezoelectric actuation can be represented as [4]:

$$[M]\{\ddot{x}(t)\}+[D]\{\dot{x}(t)\}+[K]\{x(t)\}=\lfloor F_p \rfloor\{u(t)\} \tag{1}$$

here, by defining *Ndof* as the total number of degrees of freedom of the finite element model, $[M]$, $[D]$ and $[K]$ denote $Ndof \times Ndof$ global mass, damping and stiffness matrices, respectively. $\{x(t)\}$ is the structural displacement vector of size $Ndof \times 1$. Defining L as the number of piezoelectric actuators, $\lfloor F_p \rfloor_{Ndof \times j}$ is the force matrix due to unit electric voltage from jth (j=1 to L) actuator and

$\{u(t)\}_{j\times 1}$ is the piezoelectric actuation voltage vector associated with the j[th] piezoelectric actuator. $[F_p]$ specifies the actuation characteristics of PZT actuators and depends on the types of actuators, their location on the structure and their electromechanical properties. Note that the aerodynamic and other disturbance forces are not included in Eqn. (1).

The structural matrices and the force matrix due to unit electric voltage are calculated for the smart fin by using MSC®/NASTRAN. Since MSC®/NASTRAN offers no piezoelectric coupled-field elements capability to model the piezoelectric actuators, the thermal analogy method based on the analogy between thermal strains and piezoelectric strains is used in MSC®/NASTRAN to obtain $[F_p]$. The piezoelectric strain is given by:

$$\varepsilon^p = \frac{d_{3i}}{t}\Delta V_3 \tag{2}$$

where d_{3i} is the piezoelectric strain coefficient. t and ΔV_3 represent piezoelement thickness and applied voltage respectively. Thus, the induced strain is linearly proportional to the applied voltage and similar to the thermal strain which is given by:

$$\varepsilon^{th} = \alpha_{ii}\Delta T \tag{3}$$

Substituting for the thermal coefficient α_{ii}, with $\frac{d_{3i}}{t}$, and the temperature difference ΔT, with ΔV_3, one can use the thermal analogy to simulate the piezoelectric effect:

$$\alpha_{ii} = \frac{d_{3i}}{t}, \quad \Delta T = \Delta V_3 \tag{4}$$

To simulate the voltage actuation, thermal expansion coefficients are imposed as piezoelectric strain coefficients divided by thickness and temperature change is imposed equal to the applied voltage.

3-2. Aerodynamic Model

Unsteady aerodynamic forces acting on the structure of a linear aeroelastic system can, in the frequency domain, be expressed as [5]:

$$\{F_a(x(i\omega))\} = q_\infty [Q(ik)]\{x(i\omega)\} \tag{5}$$

where ω is the frequency of the excitation. $q_\infty = \frac{1}{2}\rho V_\infty{}^2$ is the dynamic pressure where ρ is the density of air and V_∞ is the free stream velocity. $[Q(ik)]$ is the aerodynamic influence coefficient matrix and is a complex function of reduced frequency k and Mach number. $[Q(ik)]$ is calculated at several reduced frequencies for a given Mach number by using Doublet Lattice Method (DLM) available in MSC®/NASTRAN. In order to cast the dynamic aeroelastic equation of motion in a state-space form, which can be readily utilized in the modern control theories, the aerodynamic influence coefficients have to be approximated by rational functions of s (namely, fraction of

polynomials of s). There are several methods used in approximating unsteady aerodynamics using rational functions. In this study, the Roger's method is used.

The Roger's approximation to the unsteady aerodynamics is given by [6]:

$$\left[Q_{app}(ik)\right] = \left[A_0\right] + \left[A_1\right](ik) + \left[A_2\right](ik)^2 + \sum_{j=3}^{N} \frac{(ik)\left[A_j\right]}{(ik + \gamma_{j-2})} \tag{6}$$

where $\left[A_i\right]$ are real coefficient matrices to be determined such that the assumed matrix form approximates the tabulated matrices and γ_{j-2} are the aerodynamic lag parameters which are usually preselected in the range of reduced frequencies of interest. By determining the coefficients $\left[A_i\right]$ using least square error technique, approximated aerodynamic forces are obtained.

3-3. Aeroelastic Model

Introducing the approximated aerodynamic forces into Eqn. (1) and writing in the Laplace domain results in the generalized equations of motion for aeroelastic motion:

$$\begin{aligned} &\left(\left(\left[M\right] - \frac{1}{8}\rho b^2\left[A_2\right]\right)s^2 + \left(\left[D\right] - \frac{1}{4}\rho b V_\infty\left[A_1\right]\right)s + \left[K\right] - \frac{1}{2}\rho V_\infty^2\left[A_0\right]\right. \\ &\left. - q_\infty \sum_{j=3}^{N} \frac{s}{\left(s + \frac{2V_\infty}{b}\gamma_{j-2}\right)}\left[A_j\right]\right)\left\{x(s)\right\} = \left[F_p\right]\left\{u\right\} \end{aligned} \tag{7}$$

In order to improve computational efficiency, the system size is usually reduced with the modal approach. Eqn. (7) is transformed into the modal equation as follows:

$$\begin{aligned} &\left(\left(\left[\overline{M}\right] - \frac{1}{8}\rho b^2\left[A_2\right]\right)s^2 + \left(\left[\overline{D}\right] - \frac{1}{4}\rho b V_\infty\left[A_1\right]\right)s + \left[\overline{K}\right] - \frac{1}{2}\rho V_\infty^2\left[A_0\right]\right. \\ &\left. - q_\infty \sum_{j=3}^{N} \frac{s}{\left(s + \frac{2V_\infty}{b}\gamma_{j-2}\right)}\left[A_j\right]\right)\left\{\zeta(s)\right\} = \left[\overline{F}_p\right]\left\{u\right\} \end{aligned} \tag{8}$$

where

$$\left[\overline{M}\right] = \left[\phi\right]^T\left[M\right]\left[\phi\right],\ \left[\overline{D}\right] = \left[\phi\right]^T\left[D\right]\left[\phi\right],\ \left[\overline{K}\right] = \left[\phi\right]^T\left[K\right]\left[\phi\right]$$
$$\left[\overline{Q}(ik)\right] = \left[\phi\right]^T\left[Q(ik)\right]\left[\phi\right],\ \left[\overline{F}_p\right] = \left[\phi\right]^T\left[F_p\right]$$

and $\left[\phi\right]$ is the modal matrix and $\left\{\zeta(s)\right\}$ is the modal displacement vector.

Defining aerodynamic lag terms as a new augmented state such that

$$\left\{\zeta_{aj}(s)\right\} = \frac{s}{\left(s + \frac{2V_\infty}{b}\gamma_{j-2}\right)}\left\{\zeta(s)\right\} \tag{9}$$

Making use of Eqn. (9) in Eqn. (8) results in the following state-space representation of the aeroelastic system [7]:

$$\{\dot{x}\} = [A]\{x\} + [B]\{u\}$$

$$\begin{Bmatrix} \dot{\zeta} \\ \ddot{\zeta} \\ \dot{\zeta}_{a3} \\ \vdots \\ \dot{\zeta}_{a6} \end{Bmatrix} = \begin{bmatrix} [0] & [I] & [0] & \cdots & [0] \\ -[\widetilde{M}]^{-1}[\widetilde{K}] & -[\widetilde{M}]^{-1}[\widetilde{D}] & q_\infty[\widetilde{M}]^{-1}[A_3] & \cdots & q_\infty[\widetilde{M}]^{-1}[A_N] \\ [0] & [I] & -(\frac{2V_\infty}{b})\gamma_1[I] & \cdots & [0] \\ \vdots & \vdots & \vdots & \ddots & \vdots \\ [0] & [I] & [0] & \cdots & -(\frac{2V_\infty}{b})\gamma_{N-2}[I] \end{bmatrix} \begin{Bmatrix} \zeta \\ \dot{\zeta} \\ \zeta_{a3} \\ \vdots \\ \zeta_{a6} \end{Bmatrix} + \begin{bmatrix} [0] \\ [\widetilde{M}]^{-1}[\overline{F}_p] \\ [0] \\ \vdots \\ [0] \end{bmatrix} \{u\} \quad (10)$$

where $[\widetilde{M}] = [\overline{M}] - \frac{1}{8}\rho b^2[A_2]$, $[\widetilde{D}] = [\overline{D}] - \frac{1}{4}\rho b V_\infty[A_1]$, $[\widetilde{K}] = [\overline{K}] - \frac{1}{2}\rho V_\infty^2[A_0]$

The state vector $\{x\}$ consists of the modal displacement $\{\zeta\}$, modal velocity $\{\dot{\zeta}\}$ and the augmented states $\{\zeta_{aj}\}$. $[A]$ describes the system matrix and $[B]$ gives the input matrix. System matrix $[A]$ includes all aerodynamic effects such as apparent mass, aerodynamic damping and stiffness as well as structural mass, damping and stiffness. It should be noted that the system matrix $[A]$ is a function of air speed.

3-4. Verification of the Modeling Strategies

First, a normal modes analysis is performed using MSC®/NASTRAN to determine the natural frequencies and mode shapes of the smart fin. Besides the finite element analysis, open loop experiments are also performed for the determination of the structural characteristics of the smart fin. The theoretical analysis results of the natural frequencies of the smart fin are compared with the experimental ones. Table 3.1 gives a very good comparison for the first three available experimental frequencies. Figure 3.2 shows the first four theoretical mode shapes of the smart fin which are used in the current study. The first mode can be defined as the first out of plane bending mode, the second mode is predominantly torsional, the third mode is the second out of plane bending mode and the fourth mode with 108.54 [Hz] is the second torsional mode.

Table 3.1 Theoretical and experimental natural frequencies and the experimentally determined damping ratios of the smart fin

Mode number	Frequency (Hz)		Experimentally Determined Damping Ratio
	FEM	Experimental	
1	16.03	15.0	0.0190
2	47.11	50.75	0.0148
3	72.60	73.75	0.0091

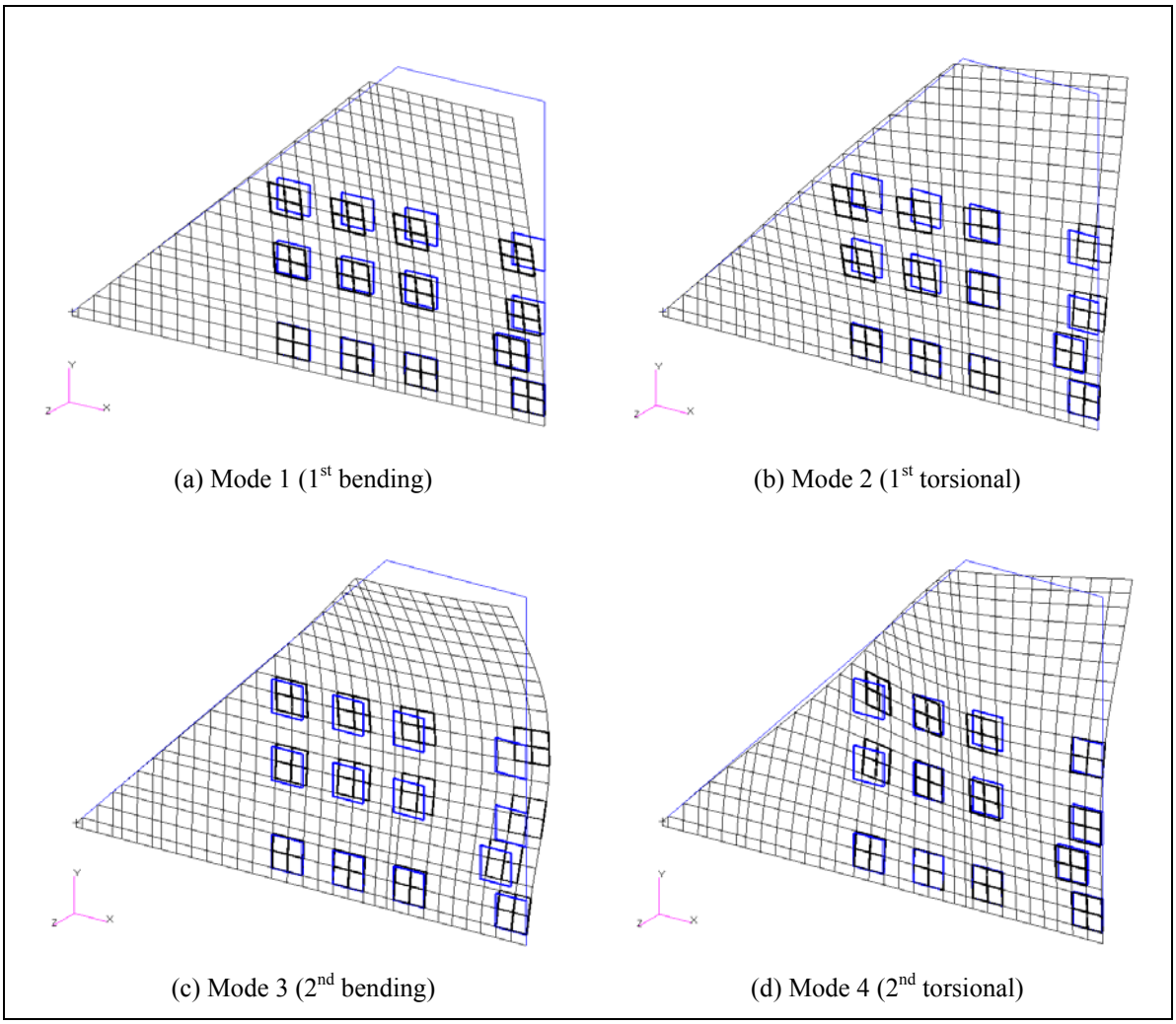

(a) Mode 1 (1st bending)

(b) Mode 2 (1st torsional)

(c) Mode 3 (2nd bending)

(d) Mode 4 (2nd torsional)

Figure 3.2 The first four mode shapes of the smart fin

Open-loop flutter analysis for the smart fin is performed at sea level by investigating the stability of the system matrix [*A*] for flight speeds ranging from 20 m/sec to 90 m/sec. The first four elastic modes are used in the analysis. Figure 3.3 shows the airspeed root-locus plot of the smart fin. The plot traces the roots of the system as the flight speed changes. The imaginary axis represents the point of neutral stability. Flutter is represented on the root-locus plot by a pole crossing this axis into the right half plane. It can be seen from the figure that the frequencies of the first aeroelastic mode (bending branch) and second aeroelastic mode (torsion branch) coalescence as the flow speed increases and the second aeroelastic mode pole crosses the imaginary axis at a speed of 84.1 m/sec and a frequency of 35.69 Hz which represents the flutter speed and the flutter frequency of the smart fin respectively. Flutter characteristics of the smart fin are also determined by using the *pk*-method of MSC®/NASTRAN. The flutter characteristics of the developed state space approach are compared with those of MSC®/NASTRAN in Table 3.2 and the results are impeccable.

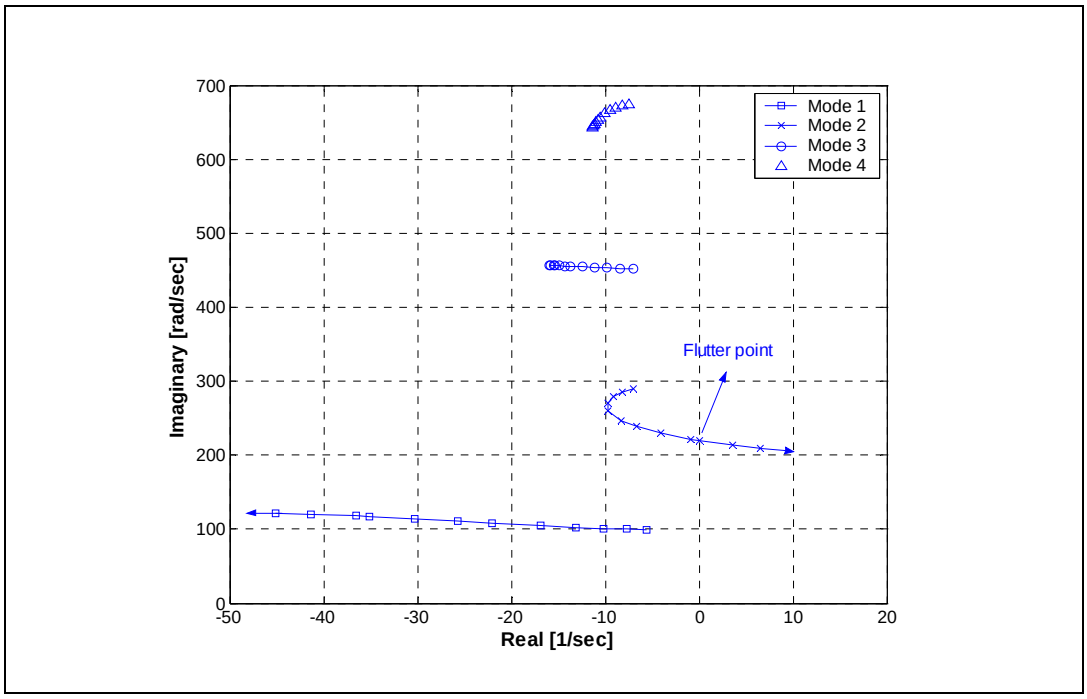

Figure 3.3 Root-locus of the state-space model of the smart fin as a function of the flight speed (ρ=1.225 kg/m^3)

Table 3.2 Comparison of the open-loop flutter characteristics

	Flutter speed (m/sec)	Flutter frequency (Hz)
MSC®/NASTRAN/Aero I	83.89	35.74
State-Space Approach	84.10	35.69
% Deviation from NASTRAN	0.25	0.14

4. CONTROL SYSTEM DESIGN

The controllers for flutter suppression of the smart fin are designed by using H_∞ synthesis. In designing a control algorithm for flutter suppression, two objectives are important. The first is to extend the flutter boundary, i.e., to use feedback control to stabilize the smart fin over a larger region of operating conditions. The second is to attenuate vibrations in the operating region where the smart fin is open-loop stable.

Figure 4.1 shows the block diagram of the interconnection structure used for controller design of the smart fin. The 2-input 2-output system model at $V_\infty = 83$ m/sec, which is quite close to the flutter boundary, is used as the nominal plant. In this MIMO model, PZT actuators are grouped into two actuator sets; actuator group 1 and group 2 as seen in Figure 2.1. The controller inputs are taken as the displacements of two points at the upper two corners of the smart fin given as Sensor 1 and Sensor 2 in Figure 2.1. The system order is reduced from 24-states to 8-states by truncating the sixteen states associated with aerodynamic lag terms. In Figure 4.1, W_{per} symbolizes the performance weight applied to output channels and ask for a reduction of the maximum singular values from all inputs to the outputs. Additive uncertainty weight W_{add} and the uncertainty set Δ_{add} represent additive uncertainty which is used to account for model variations in the low frequencies and unmodeled dynamics at higher frequencies. The magnitude plots of the selected additive and performance weighting functions are presented in Figure 4.2. The same scales are used for two channels of weights

W_{add} and W_{per}. In addition to the additive uncertainty, parametric uncertainty is added to the system to take into account the movement of the dominant pole as flight speed increases. Since the damping value of the flutter mode varies significantly without the frequency change near the flutter point, the system matrix is transformed into bi-diagonal form and only the damping term is treated as the parametric uncertainty [8]. Additive and parametric uncertainties provide that the closed-loop system meets the stability objectives, increasing the flutter boundary above its open-loop value while maintaining stability for lower velocities. The constant actuator weight $W_{act} = diag(0.01, 0.01)$ is chosen to limit the voltage applied on the piezoelectric actuators. Sensor noise $W_{noise} = diag(0.05, 0.05)$ is added to the feedback signals to corrupt the measurements.

H_∞ controller is designed according to the defined performance and uncertainty specifications by using MATLAB® Robust Control Toolbox [9], and a 18th-order controller is obtained. A balanced realization of the controller is then obtained, and the 9 states are truncated from the system. The resulting 9-state controller differs in H_∞ norm from the full-order controller by less than 1%.

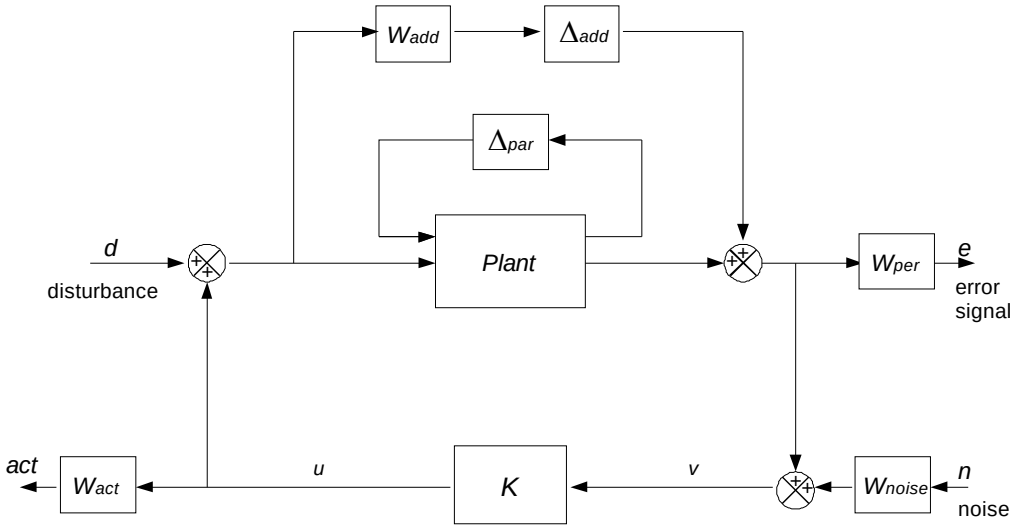

Figure 4.1 Control design block diagram for the smart fin

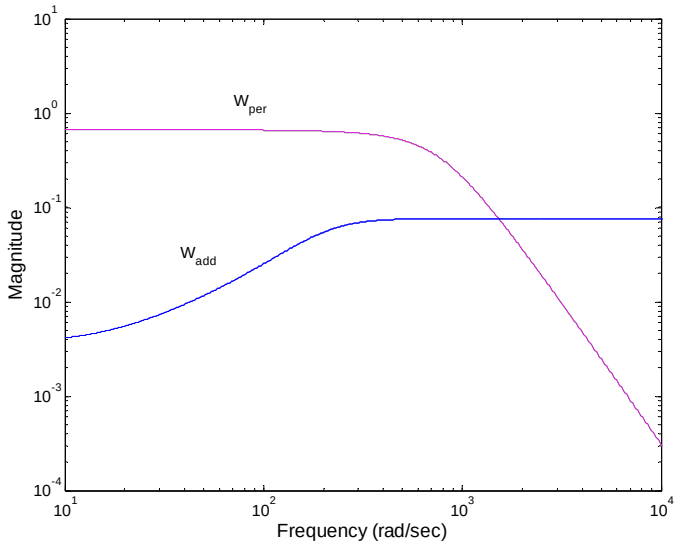

Figure 4.2 Additive and performance weights

5. RESULTS

The comparison of the frequency responses at the flow speed of 83 m/sec for both uncontrolled and controlled cases is given in Figure 5.1. The controller is simulated on the full-order (24th order) system model. It can be seen that the application of H_∞ controller is successful in eliminating vibrations at the first two aeroelastic modes, especially where the flutter is likely to occur. Figure 5.2 shows the open and closed-loop magnitude plots at 70 m/sec, which is quite below the flutter speed. The closed-loop system still results in successful suppression of the oscillations even at speeds lower than the flutter speed.

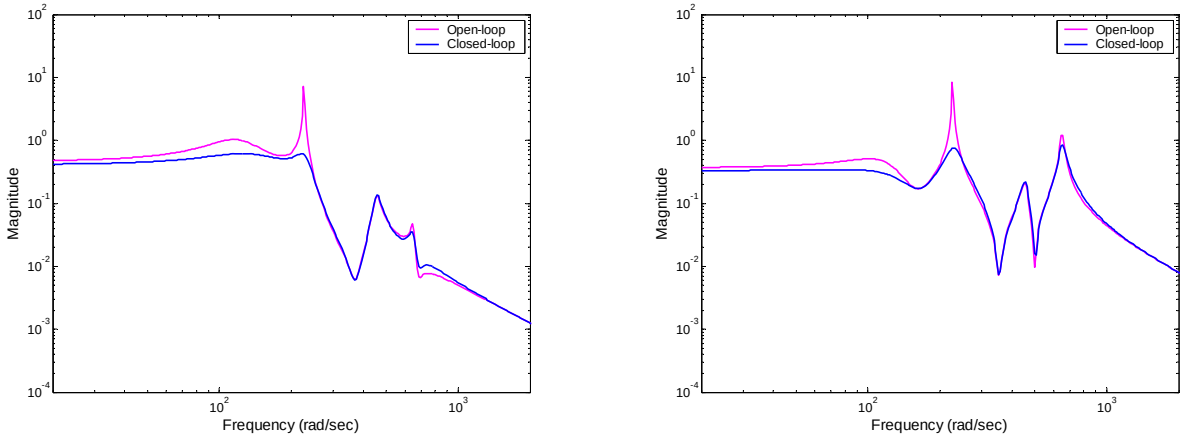

Figure 5.1 Flutter suppression results for Sensor 1 signals at a speed of 83 m/sec Control signal is from (a) PZT actuator group 1 (b) PZT actuator group 2

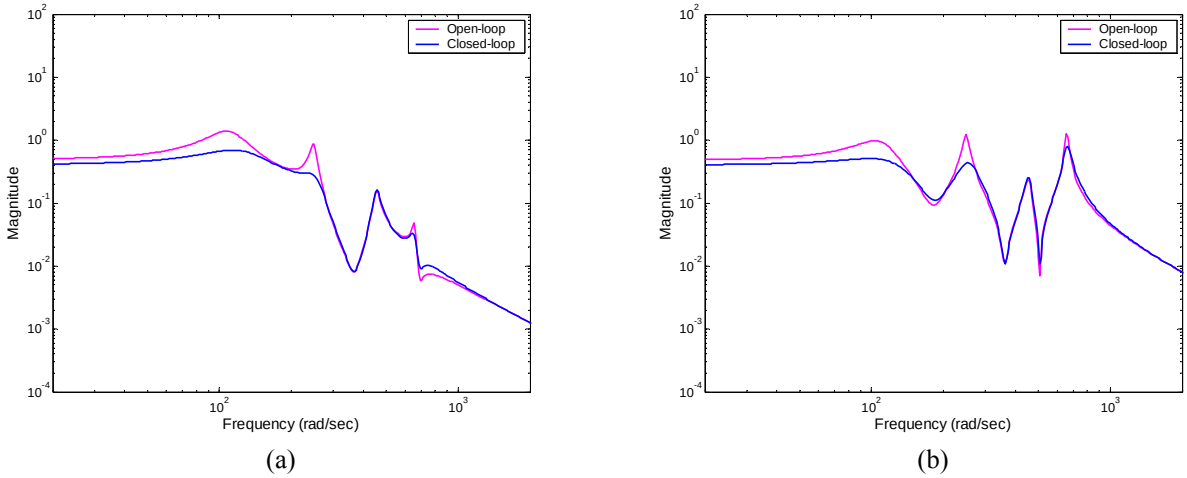

Figure 5.2 Flutter suppression results for Sensor 1 signals at a speed of 70 m/sec Control signal is from (a) PZT actuator group 1 (b) PZT actuator group 2

The flutter speed is found to increase to 93.7 m/sec (11.4% enhancement in the flutter boundary) for the MIMO model by using H_∞ controller. When the smart fin is excited by using all the PZT actuators on one face and the control input is selected as Sensor 1 signals, the system becomes SISO model. In this case, the flutter speed is determined to increase to 88.6 m/sec (5.4% flutter enhancement). The reason for the lower performance in the SISO model is due to the lack of the torsional control force.

6. CONCLUSIONS

This study presented a numerical approach developed for the active flutter control of a smart fin. In the controller design, the additive uncertainty was used to cover the differences between the system models in the low frequencies and unmodeled dynamics at higher frequencies. The parametric uncertainty model was used to take into account the system changes with respect to varying airspeed. The designed H_∞ controllers showed improved behavior over a wide flow speed range. The developed controllers effectively suppressed the fluttering vibrations and improved the flutter speed of the smart fin.

ACKNOWLEDGEMENTS

This work was partially supported by TUBITAK (Turkish Scientific and Technological Research Center). The first author gratefully acknowledges the support given. This work was also partially supported by NATO/RTO/Applied Vehicle Technology Panel through the project 'T-133, Development and Verification of Various Strategies for the Active Vibration Control of Smart Aerospace Structures Subjected to Aerodynamic Loading'. The authors gratefully acknowledge the support given.

REFERENCES

1. Heeg, J., "Analytical and Experimental Investigation of Flutter Suppression by Piezoelectric Actuation", NASA TP 3241 (February 1993).
2. Döngi, F., Dinkler, D., and Kröplin, B., "Active Panel Flutter Suppression Using Self-Sensing Piezo Actuators", *AIAA Journal*, Vol. 34, p: 1224-1230 (June 1996).
3. Han, J. H., Tani, J., and Qiu, J., "Active Flutter Suppression of a Lifting Surface Using Piezoelectric Actuation and Modern Control Theory", *Journal of Sound and Vibration*, Vol. 291, p: 706-722 (2006).
4. Bandyopadhyay, B., Manjunath, T.C., Umapathy, M., "Modeling, Control and Implementation of Smart Structures: A FEM–State Space Approach", Springer, Berlin Heidelberg (2007).
5. ZAERO, "Theoretical Manual", Version 8.0, ZONA Technology Incorporation (July 2007).
6. Roger, K.L., "Airplane Math Modeling and Active Aeroelastic Control Design", AGARD-CP-228, p: 4.1– 4.11 (1977).
7. Karadal, F. M., "Active Flutter Suppression of a Smart Fin", *M.Sc. Thesis*, Middle East Technical University (September 2007).
8. Vipperman, J. S., Barker, J. M., Clark, R. L., and Balas, G. J., "Comparison of μ - and H_2-Synthesis Controllers on an Experimental Typical Section", *Journal of Guidance, Control and Dynamics*, Vol. 22, p: 278-285 (1999).
9. Balas, G. J., Chiang, R., Packard, A. and Safonov, M., "Robust Control Toolbox User's Guide", The MathWorks Inc. (2006).
10. Sensor Technologies Limited, *Product Data Sheets* (2002).

APPENDIX

This appendix gives the electromechanical and material properties of BM500 type [10] PZT patches used in the study.

Piezoelectric strain constant matrix:

$$[d] = \begin{bmatrix} 0 & 0 & 0 & 0 & 0 & 5.4425 \\ 0 & 0 & 0 & 0 & 5.4425 & 0 \\ -1.6538 & -1.6538 & 3.6012 & 0 & 0 & 0 \end{bmatrix} \times 10^{-10} \text{ [m/V]}$$

Elastic stiffness coefficient matrix:

$$[c] = \begin{bmatrix} 12.1 & 7.54 & 7.52 & 0 & 0 & 0 \\ 7.54 & 12.1 & 7.52 & 0 & 0 & 0 \\ 7.52 & 7.52 & 11.1 & 0 & 0 & 0 \\ 0 & 0 & 0 & 2.11 & 0 & 0 \\ 0 & 0 & 0 & 0 & 2.26 & 0 \\ 0 & 0 & 0 & 0 & 0 & 2.26 \end{bmatrix} \times 10^{10} \text{ [N/m}^2\text{]}$$

Density:

$$\rho = 7650 \text{ kg/m}^3$$